Combustion and Flame 177 (2017) 1–9

Contents lists available at ScienceDirect

Combustion and Flame

journal homepage: www.elsevier.com/locate/combustflame

Reaction mechanisms of potassium oxysalts based energetic composites

Wenbo Zhou[a,b], Jeffery B. DeLisio[a,b], Xizheng Wang[a,b], Michael R. Zachariah[a,b,*]

[a] Department of Chemical and Biomolecular Engineering, University of Maryland, College Park, MD 20742, USA
[b] Department of Chemistry and Biochemistry, University of Maryland, College Park, MD 20742, USA

ARTICLE INFO

Article history:
Received 6 August 2015
Revised 28 August 2015
Accepted 26 May 2016

Keywords:
Ignition temperature
Oxygen release
Melting
Oxysalts
Reaction mechanism

ABSTRACT

Ignition temperature is a simple and important parameter that pertains to both the practical aspects of thermite usage as well as a key to exploring reaction mechanisms. In this study, nine aluminum-fueled oxysalt-containing thermites including $K_2S_2O_8$, K_2SO_4, KIO_4, KIO_3, $KClO_4$, $KClO_3$, $KBrO_3$, KNO_3 and K_3PO_4, were investigated. Results from combustion cell tests show that these thermites can be divided into two groups, with the reactive thermites (e.g., Al–$K_2S_2O_8$) generating ~10× higher of pressure and ~10× shorter of burn time than the less reactive thermites in the aforementioned list (e.g., Al–K_2SO_4). Thermal decomposition analysis of these oxysalts at both slow and fast heating rates (0.17 K/s v.s. 10^5 K/s) demonstrates that these oxysalts have a wide range of oxygen release and melting temperatures. On the other hand, the ignition temperatures of the reactive thermites (in Ar and air) are consistent with the temperature of polymorphic phase change of alumina (close to the melting point of Al), indicating that the limiting initiation step of these thermites is the acceleration of outward diffusion flux of Al. In addition, the ignition temperatures of these reactive thermites in vacuum are much higher than those in Ar, suggesting that ignition is based on the interaction between outwardly diffused Al, and generated gas phase O_2. In contrast, the ignition temperatures of the two less reactive thermites are insensitive to pressure. They ignite at temperatures much higher than the melting point of Al, although lower than the decomposition temperature of the corresponding oxysalts, indicating a condensed phase reaction mechanism. Finally, by employing carbon as a non-melting, non-oxide coated fuel, we found an essentially direct correlation between the oxygen release temperature and the ignition temperature.

1. Introduction

Since the thermite reaction was first named by Goldschmidt in 1908 [1], the concept has been currently broadened to a variety of exothermic reactions involving a metal reacting with an oxide (metal or non-metal) or an oxysalt [2–5]. Due to its extremely high energy density, the thermite system has been employed in a wide array of applications in the pyrotechnic, metallurgical, and ceramic industries [2–5], which has prompted studies to improve their utilization by tailoring their combustion and ignition behaviors [6–10]. The latter property also involves practical safety concerns related to the large-scale industrial use [11,12]. One important research direction is to improve the ignitibility of thermites, which is affected by many factors (contact area, chemical composition, hygroscopicity, etc.). The most common method is by increasing the contact area between the fuel and oxidizer, which can reduce the diffusion distance of reactive species to permit ignition at lower temperatures [13–17]. This higher degree of intimacy can be achieved by either decreasing the particle size [14–17], better mixing [13,18,19], or increasing the particle porosity [20].

For the most common aluminum-fueled thermite systems, ignition was proposed to be initiated by a solid-state reaction [21]. Subsequent reaction requires movement of reactive species towards each other, although the nature of this movement is subject to considerable debate [22–28]. However, it was previously reported that the prerequisite for ignition is the availability of molten aluminum [21,29]. Based on this speculation, ignition temperatures for a plethora of thermites should be around the melting point of aluminum. However, a recent study by Jian et al. [30] shows that there can be large differences in ignition temperatures among different nano-thermite formulations involving aluminum and metal oxides. For instance, some formulations (e.g., Al–Bi_2O_3, Al–SnO_2) have ignition temperatures lower than both the melting point of aluminum, and the decomposition temperatures of oxidizers, suggesting another condensed phase reaction

* Corresponding authors at: Department of Chemical and Biomolecular Engineering, and Department of Chemistry and Biochemistry, University of Maryland, College Park, MD 20742, USA.
E-mail address: mrz@umd.edu (M.R. Zachariah).

http://dx.doi.org/10.1016/j.combustflame.2016.05.024
0010-2180/

mechanism that is not governed by melted aluminum [31]. Similarly, Dean et al. [32] examined another nano-thermite formulation (Al–NiO), which produces minimal gas upon ignition, with a much lower ignition temperature (~400 °C) [33] than either the melting temperature of Al or the decomposition temperature of NiO. Sullivan et al. [34] implemented in situ rapid heating microscopy to monitor the nano-thermite reaction of Al–WO_3 and found a reactive sintering phenomenon [35] in which no gas was released, and the reactants deformed to maximize intimate surface contact. While several thermites appear to react via this condensed phase route [32–37], ignition temperatures of some other formulations may exceed the decomposition temperature of metal oxides, suggesting a different reaction mechanism [30].

To date, discussions on ignition mechanism of thermites have been limited to formulations containing various metal oxides (CuO, Fe_2O_3, *etc.*), whereas the ignition mechanism for thermite formulations containing oxysalts (nitrates [38–40], (per)chlorates [41–44], (per)iodates [45–47], *etc.*) have not been explicitly studied from a mechanistic standpoint. Typically, Al–oxysalt thermites exhibit lower ignition temperatures and higher reaction rates [44,47–49], which are associated with the low oxygen release temperatures of the corresponding oxysalts. An initial exothermic decomposition of some oxysalts during heating may also contribute to the low ignition temperature [41,47]. Recently, a new formulation based on persulfates was found to be more reactive when compared to other oxysalts [50]. The superiority of oxysalts in thermite performance can likely be attributed to the higher oxygen content, and the lower bond energy of the nonmetal-oxygen pair in oxysalts when compared to the metal–oxygen pair in metal oxides [50]. Of particular interest is whether the ignition temperature (T_{ig}) is a predictable function of the oxygen release temperature (T_{O_2}), the melting temperature of aluminum ($T_{Al\text{-}melt}$), and the melting temperature of oxidizer ($T_{oxidizer\text{-}melt}$).

In this paper, we systematically investigated the ignition of thermites that involve Al and a variety of potassium oxysalts, in relation to the physiochemical changes of these components during heating. These studies involved using constant-volume combustion cell tests, thermal decomposition tests for oxysalts under both slow heating (10 K/min) and ultrafast heating (~10^5 K/s) conditions, and ignition tests for both microscale and nanoscale thermites in air, in Ar and in vacuum. Nano-carbon-fueled thermites containing similar oxysalts were also used as controls to tweeze out the role of liberated oxygen.

2. Material and methods

2.1. Materials

Nano-sized aluminum was obtained from Argonide Corporation, and nano-sized carbon black was obtained from Cobot Corporation. Both materials have an average size of ~50 nm. Micro-sized potassium persulfate ($K_2S_2O_8$) powders were purchased from Fluka. All of the other micro-sized oxysalt powders, namely potassium sulfate (K_2SO_4), potassium nitrate (KNO_3) potassium chlorate ($KClO_3$), potassium perchlorate ($KClO_4$), potassium bromate ($KBrO_3$), potassium iodate (KIO_3), potassium periodate (KIO_4), and potassium phosphate (K_3PO_4) were purchased from Sigma-Aldrich. Scanning electron microscopy (SEM, Hitachi, SU-70 FEG-SEM) analysis shows that these as-received potassium oxysalts powders have a wide range of sizes from 1 µm to 100 µm.

The corresponding nine nano-sized potassium oxysalts were prepared by an aerosol spray drying process, as is shown in Scheme 1. In short, 0.02 mol/L water solution of oxysalt was prepared in the atomizer and sprayed into 1 µm droplets by a pressured air flow. Droplets flowed through a diffusion dryer to remove most of the water, followed by complete dehydration by a tube furnace at 150 °C for $K_2S_2O_8$ and at 180 °C for the other oxysalts. The dehydrated nanoparticles were finally collected on a Millipore membrane filter with a pore size of 0.4 µm. The average size of nine nano-oxysalts is ~0.5 µm. Particle sizes were measured by SEM and statistically analyzed from a random selection of 60 particles in SEM images.

To prepare the thermite composite, nano-fuels (Al or C) were mixed with oxysalts (microscale or nanoscale) in a stoichiometric ratio. Accounting for the alumina shell (30%) on the nano-Al, the actual weight of nano-Al added was 1.4 times higher. The mixture was then sonicated in hexane for 30 min and then the solvent was evaporated at room temperature.

2.2. Constant-volume combustion characterization

The analysis of nano-Al/micro-oxysalt thermite reactions was conducted in a constant-volume combustion cell (Scheme 1). Prior to tests, all the thermite samples were dried in vacuum for hours in order to mitigate the adverse influence of hygroscopicity. 25 mg of thermite sample was loaded inside the combustion cell that has an internal spacing of ~13 cm^3. After igniting the sample with a heated nichrome coil, the temporal pressure and optical emission from the thermite reaction were electronically recorded.

2.3. TG-DSC analysis of the decomposition of oxysalts

Thermogravimetry and differential scanning calorimetry (TG-DSC) tests of microscale oxysalts were conducted simultaneously in a SDT Q600 from TA Instruments, USA. Around 2 mg of as-received oxysalt powders was loaded into the sample crucible inside the apparatus and heated at 10 K/min in 100 L/min Ar flow. The TG and DSC heat flow calibrations were conducted prior to tests. For the TG calibration, two calibration weights were used to calibrate the beam and weight correction factors. For the DSC heat flow calibration, the capacity curve of sapphire over the range of 500–1800 K, as well as the heat of fusion of high purity zinc metal, were analyzed and compared with the standard values to generate a calibration cell constant. In the analysis of the TG-DSC results, the onset temperatures of physicochemical changes (including phase and chemical changes) are defined as the crossing points of extrapolated curves.

2.4. T-jump TOF-MS analysis of the decomposition of oxysalts

The decomposition of oxysalts (microscale or nanoscale) at ultrafast heating rates of 4×10^5 K/s was investigated via temperature-jump time-of-flight mass spectrometry (T-jump TOF-MS, in-house assembled). A concentrated oxysalt powder suspension in hexane was deposited onto a 76 µm Pt wire uniformly, to a thickness < 10 µm so that the temperature of the deposit is approximated by the wire temperature. The loaded Pt wire was then inserted into the MS chamber and rapidly joule-heated to ~1400 K by a 3 ms pulse. The temporal temperature of the wire was measured from the detected current and voltage according to the Callender–Van Dusen equation [51]. TOF-MS spectra was collected every 0.1 ms. A detailed experimental description can be found in Ref. [52]. In the analysis of the MS results, the onset temperature of a specific species is defined based on 5% of the maximum intensity of its MS peak.

2.5. Ignition tests of thermite reactions

A Vision Research Phantom v12.0 high speed camera (14.9 µs per frame) was employed to determine the onset of ignition on the wire. By mapping the temporal optical emission from the high-speed imaging, and the temporal wire temperature, the ignition

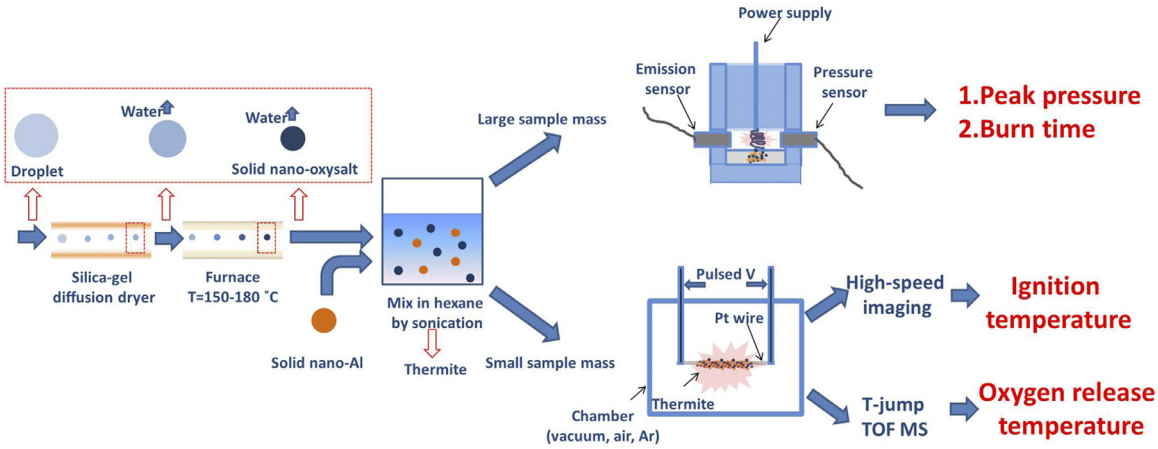

Scheme 1. The experimental flow chart including spray drying process for sample preparation, a pressure cell for detecting pressure and optical emission from thermite reaction, and a pulsed wire heating set-up coupled with T-jump TOF-MS and high-speed camera for detecting characteristic temperatures.

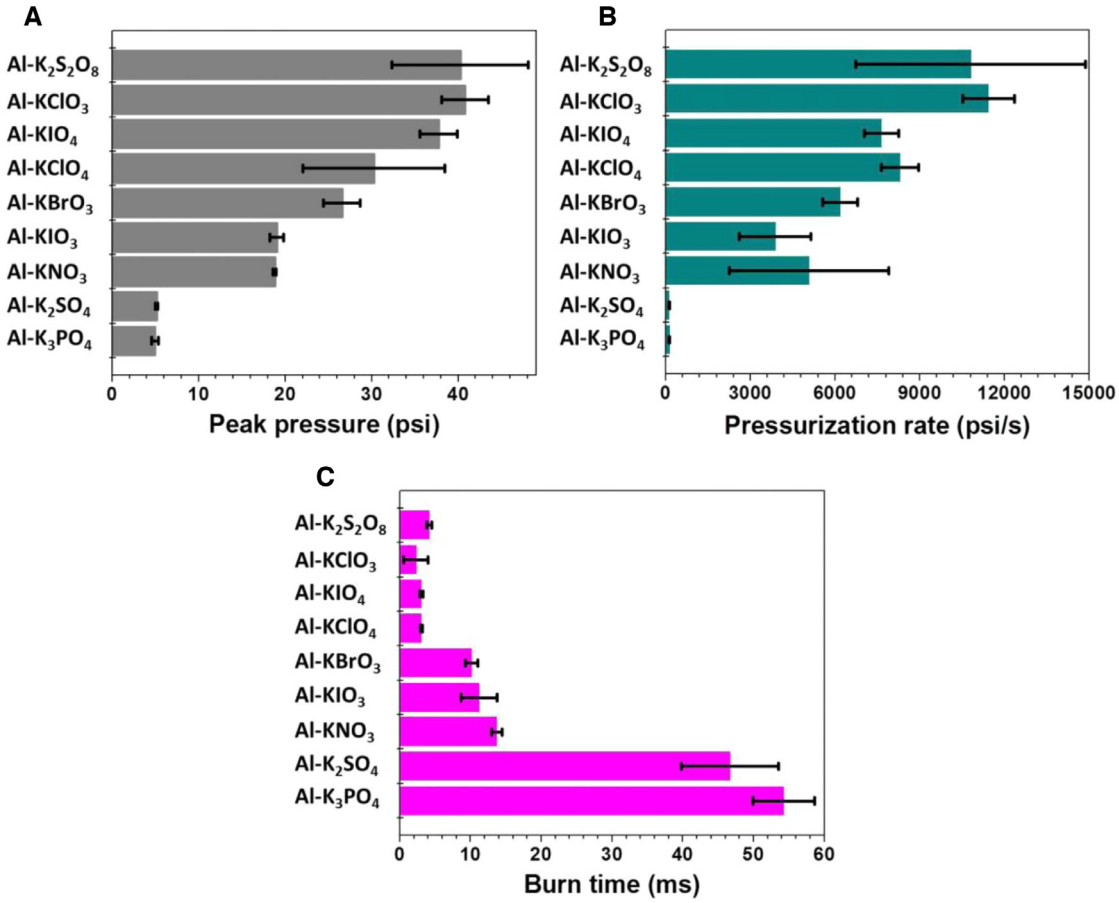

Fig. 1. Maximum pressure (A), pressurization rate (B), and burn time (C) for thermite reactions between nano-Al and micro-oxysalts. 25 mg thermite sample was employed in each constant volume combustion cell test. Errors bars represent at least two experiments in parallel.

temperatures of thermites were identified as the points where light intensities begin to rise. These experiments were carried out in vacuum, air or Ar.

3. Results and discussion

3.1. Reactivities of oxysalts in nano-aluminum-fueled thermites

We begin with the combustion performance of the nine Al–oxysalt thermites, in the combustion cell test. Figure 1 shows the maximum pressures, pressurization rates, and burn times (the full-width half-maximum of the optical emission curve) for the thermite reactions between nano-Al and micro-oxysalts. Also apparent in Fig. 1 is the very wide range in performance, with the maximum peak pressures for Al–$K_2S_2O_8$, Al–$KClO_3$, Al–KIO_4 and Al–$KClO_4$ being more than six times larger than those of Al–K_2SO_4 and Al–K_3PO_4 (Fig. 1A), indicating that the former four thermites generated more gas during reaction. A similar result in the pressurization rate was shown for these thermite reactions, with the rates in thermites that release extensive gas (Al–$K_2S_2O_8$, Al–$KClO_3$,

Table 1
Summary of the amount of gas generation, major gas species, adiabatic temperature and reaction heat from the Al–oxysalt thermite reactions. Thermodynamic data were calculated based on a constant enthalpy and pressure equilibrium using CHEETAH. The fuel and oxidizer were mixed in a stoichiometric ratio.

Formulations	cc gas/g[a]	Major gas products (mol%)	Adiabatic temperature (K)	Standard reaction heat (kJ/g)[b]
Al+KNO_3	4.0×10^3	K (49%), N_2 (24%), Al_2O_3 (25%)[c]	3732	−7.6
Al+$KClO_3$	4.1×10^3	KCl (55%)[d], Al_2O_3 (35%)[c]	3791	−9.8
Al+$KClO_4$	4.2×10^3	KCl (46%)[d], Al_2O_3 (44%)[c]	3842	−10.6
Al+$KBrO_3$	3.4×10^3	KBr (64%)[d], Al_2O_3 (34%)[c]	3789	−7.7
Al+KIO_3	2.5×10^3	KI (79%)[d], Al_2O_3 (20%)[c]	3686	−5.7
Al+KIO_4	2.9×10^3	KI (64%)[d], Al_2O_3 (35%)[c]	3796	−6.9
Al+K_2SO_4	4.7×10^2	K (66%), SO_2 (27%)	2040	−3.9
Al+$K_2S_2O_8$[e]	–	–	–	−5.8
Al+K_3PO_4[e]	–	–	–	−0.9

[a] cc = cubic centimeters.
[b] The standard reaction heat (kilojoules per gram of thermite) was calculated for formulations with fuel/oxide in a stoichiometric ratio in the 1 atm, 298 K condition. The reaction equations were shown in eq. S1–S9, and also in Fig. S1. The standard heat of formation for each reaction/product (Table S1) was used to calculate the reaction heat.
[c] Al_2O_3 here is not molecular Al_2O_3. It involves decomposition into several gaseous products (e.g., O_2, O, AlO).
[d] KX (X=Cl, Br, I) involve gaseous KX, K, and X.
[e] The combustion temperature and gas generation for $K_2S_2O_8$ and K_3PO_4 were not found in CHEETAH.

Al–KIO_4 and Al–$KClO_4$) more than one order of magnitude larger than the rates in less gas generating thermites (Al–K_2SO_4 and Al–K_3PO_4) (Fig. 1B). Not surprisingly, we also observed a general relationship of higher peak pressure or pressurization rate corresponding to a shorter burn time (Fig. 1C). The differences in these reaction characteristics indicate that the Al–oxysalt thermite reactivity, as is reflected from the scale of pressurization rate and burn time, is correlated to the capability of the relevant oxysalt to generate gas. Based on these results, the nine thermites can be divided into two groups: the reactive thermites (Al–$K_2S_2O_8$, Al–KIO_4, Al–KIO_3, Al–$KClO_4$, Al–$KClO_3$, Al–$KBrO_3$ and Al–KNO_3) and the less reactive thermites (Al–K_2SO_4 and Al–K_3PO_4).

The combustion performance of some of these Al–oxysalt thermites was also assessed by thermodynamic equilibrium calculation as summarized in Table 1. The amount of gas generation, major gas species, adiabatic flame temperature, and reaction heat were calculated using CHEETAH software for constant pressure and enthalpy. The Al and oxysalts were mixed in a stoichiometric molar ratio, without consideration of additional oxide shell on the Al particles. Table 1 shows that there is a correlation between gas generation and thermite reactivity. While a larger amount of gas generation ($\sim10^3$ cc/g) corresponds to a higher adiabatic flame temperature (>3700 K) and reaction heat (<−6 kJ/g) (e.g. $KClO_3$ and $KClO_4$), poor gas generation ($\sim10^2$ cc/g) corresponds to a lower adiabatic flame temperature (<2100 K) and reaction heat (>−4 kJ/g) (e.g. K_3PO_4 and K_2SO_4). The results on the amount of gas generation are consistent with the peak pressure from the combustion cell test (Fig. 1A), demonstrating that the difference in total gas volumes generated from reactive (Al–KIO_4) and less reactive (Al–K_2SO_4) thermites can be as large as 1 order of magnitude.

3.2. Thermal decomposition of oxysalts at slow heating rates (10 K/min)

Since the gas generation appears to be correlated to the reactivity of oxysalt-containing thermites (Fig. 1), the thermal decomposition of neat microscale oxysalt powders was examined to identify the species and the temperature of gas evolution. TG-DSC results (Fig. S1) demonstrate that these oxysalts show different onset temperatures of physicochemical changes. The primary thermal results for onset temperature, gas release, and product identification are summarized in Table 2. In general, all of the nine oxysalts generate O_2 at different stages, with $K_2S_2O_8$ showing the lowest O_2 generation temperature, while K_2SO_4 and K_3PO_4 release O_2 at temperatures several hundreds of Kelvin higher than the other oxysalts. In relation to the corresponding thermite reactions (Fig. 1A), we find that the oxysalt having a low O_2 release temperature usually corresponds to a thermite event with a high pressure and faster overall reaction (also see Fig. S2 for the relationships between O_2 release temperature and peak pressure (Fig. S2A) or pressurization rate (Fig. S2B)). This indicates that the oxygen release temperature is a good metric for evaluating oxysalt-containing thermites.

It is interesting to note that many oxysalts in Table 2 have a melting temperature lower than the O_2 release temperature. Considering the much higher oxygen mobility in a melt, a melting event commencing prior to thermal decomposition (O_2 release) may also have a potential impact on initiating the thermite reaction.

3.3. Thermal decomposition of oxysalts at ultrafast heating rates (4×10^5 K/s)

In order to investigate oxygen release at heating rates that more closely represent a combustion event, T-jump TOF-MS at a heating rate of 4×10^5 K/s was employed, and the onset temperatures for corresponding generated gases were determined. As an example, the overall temporal MS intensity of molecular oxygen released from $K_2S_2O_8$ is shown in Fig. 2 together with the temporal temperature trace. In comparison to the result in TG-DSC tests (10 K/min), the O_2 release temperature of microscale $K_2S_2O_8$ powders increased by only a small amount (~50 K) at ultrafast heating rates ($\sim10^5$ K/s) (Fig. 2). All of the other microscale oxysalts similarly release O_2 at temperatures of 30–100 K higher (Fig. 3 and Table S2). The MS results (Fig. 2) enable us to link the O_2 release temperature to the corresponding ignition temperature as will be discussed in the next section.

3.4. T-jump ignition temperature

Ignition temperatures of the nine oxysalts were determined from the optical emission profiles. For example as shown in Fig. 2, the ignition temperature of nano-Al/micro-$K_2S_2O_8$ in Ar was measured to be 893 K as the onset of optical increase. Given that this ignition temperature is ~270 K higher than the O_2 release temperature (Fig. 2), we previously speculated that the O_2 release is one of the prerequisites for ignition, while it does not determine the initiation of Al–$K_2S_2O_8$ reaction [50]. We raise an important question in this study as to whether O_2 release prior to ignition is necessary for the initiation of the other Al–oxysalt reactions.

Table 2
Summary of the thermal decomposition events of oxidizers during heating (10 K/min). The onset temperature and relevant products in each event are listed. The parentheses show the melting phase change of oxidizers.

Oxidizers	Temperature (K)	Events	Products	Temperature (K)	Events	Products
$K_2S_2O_8$	556	Decomposition	$K_2S_2O_7$, O_2	725	Decomposition	K_2SO_4, O_2, SO_2[a]
K_2SO_4	1357	Melting	K_2SO_4 (l)	1394	Decomposition	K, O_2, SO_2[b]
KIO_4	613	Decomposition	KIO_3, O_2	797	Decomposition	KI, O_2[c]
KIO_3	809	Decomposition	KI, O_2[c]	–	–	–
$KClO_4$	877	Melting	$KClO_4$ (l)	895	Decomposition	KCl, O_2[c]
$KClO_3$	695	Melting	$KClO_3$ (l)	745	Decomposition	KCl, O_2[c]
$KBrO_3$	680	Melting	$KBrO_3$ (l)	699	Decomposition	KBr, O_2[c]
KNO_3	601	Melting	KNO_3 (l)	913	Decomposition	K, O_2, NO_2[d]
K_3PO_4	1347	Melting	K_3PO_4 (l)	1539	Decomposition	K_2O, P, O_2[e]

[a] The final products from the decomposition of $K_2S_2O_8$ are referred to [50].
[b] The final products from the decomposition of K_2SO_4 are referred to [53].
[c] The final products from the decomposition of KIO_3, KIO_4, $KClO_3$, $KClO_4$ and $KBrO_3$ are measured from our TG-DSC results (Fig. S1).
[d] The final products from the decomposition of KNO_3 are referred to [54].
[e] The final products from the decomposition of K_3PO_4 are referred to [55].

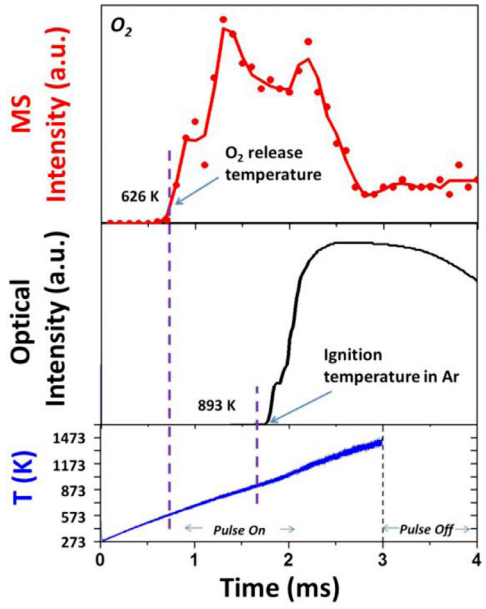

Fig. 2. Temporal oxygen release from $K_2S_2O_8$ decomposition, and temporal optical emission from Al–$K_2S_2O_8$ reaction under ultrafast heating (4×10^5 K/s). The bottom panel shows the temporal temperature trace from the Pt wire. The middle panel shows the temporal trace of optical intensity from the thermite reaction in Ar, with the designated ignition temperature (893 K). The top panel shows the temporal MS intensity of oxygen release from the decomposition of $K_2S_2O_8$, with the onset temperature at 626 K.

To address this issue, we compared the O_2 release temperatures and ignition temperatures of all the nine nano-Al/micro-oxysalt thermites in Fig. 3. Figure 3A shows that although Al–KNO_3, Al–$KClO_4$, Al–KIO_3, Al–$KClO_3$, Al–$KBrO_3$, Al–KIO_4, and Al–$K_2S_2O_8$ have different O_2 release temperatures, they all ignited around the same temperature in Ar, and nominally ~50 K below the melting point of Al. Furthermore, ignition appears to be insensitive to available gas phase oxygen since the ignition temperature in Ar and air appear to be similar. The dotted vertical line in the plot (Fig. 3A) corresponds to the melting point of aluminum, and it appears that most of the ignition temperatures are aligned vertically and parallel to the dotted line, and thus do not correlate with the O_2 release temperature. These results imply that the ignition of the Al–oxysalt thermites is dominated by the accelerated outward diffusion of Al when approaching its melting point. The generated O_2 concentration locally from the decomposition of oxysalts is much higher than that in air (see supplemental information for the detailed comparison of the O_2 concentrations in film and in air), so that the effect of O_2 in air is minimal to the ignition temperature of reactive Al–oxysalt thermites (Fig. 3A). However, when ignited in vacuum, these thermites show strikingly increased and distinct ignition temperatures (Fig. 3B). Gaseous oxygen generated from the oxysalt will presumably have little time to interact with Al in vacuum (see supplemental information for the detailed estimation of the O_2 residence time in thermite film both in air and in vacuum), therefore the delayed and thus higher temperature ignition in vacuum should be attributed to condensed phase transfer of oxygen.

The constant ignition temperature for these Al–oxysalt thermites at ~880 K corresponds to a critical phase change in the Al particle shell from amorphous (< 880 K) to γ-alumina [22]. Trunov et al. reported that the density of γ-alumina is larger than amorphous alumina, thus the newly formed γ-alumina at ~880 K was not able to form a continuous dense layer outside the Al particle [22]. This partially covered shell facilitates the accelerated diffusion of Al, resulting in the increased oxidation rate of Al, which from the perspective of ignition, refers to the consistent ignition temperature for the reactive Al–oxysalt thermites at ~880 K.

The reaction behavior of Al–K_2SO_4 and Al–K_3PO_4 thermites is clearly very different from the other seven thermites. Figure 3A shows that their ignition temperatures in Ar are more than 100 K higher than the melting temperature of Al. In this case, Al is completely melted and most likely in intimate contact with the oxysalt. Considering that their O_2 release temperatures are even higher than their ignition temperatures, the ignition of Al–K_2SO_4 an Al–K_3PO_4 thermites presumably follows a condense phase route similar to the aforementioned case for the other thermites in vacuum (Fig. 3B). This postulated condense phase reaction mechanism for Al–K_2SO_4 and Al–K_3PO_4 thermites is further confirmed by their unchanged ignition temperatures in vacuum (Fig. 3B). However, when ignited in air, both Al–K_2SO_4 and Al–K_3PO_4 thermites show decreased ignition temperatures approaching the melting temperature of Al (Fig. 3A). This is consistent with these oxysalts acting almost as dead weight and the aluminum penetrating the alumina shell above its melting point to ignite with gaseous oxygen.

We also conducted similar experiments by decreasing the dimension of oxysalts to nanometer scales so that the contact area between the fuel and oxidizer can be significantly increased. The motivation of this control experiment is to further evaluate our proposed reaction mechanism that includes reactive gaseous oxygen. Fig. S3 and Table S3 show a consistent correlation between ignition temperatures of the nano-Al/nano-oxysalt thermites in Ar, air and vacuum, similar to Fig. 3 for nano-Al/micro-oxysalt thermites. To understand the effect of the powder size of oxysalts, a

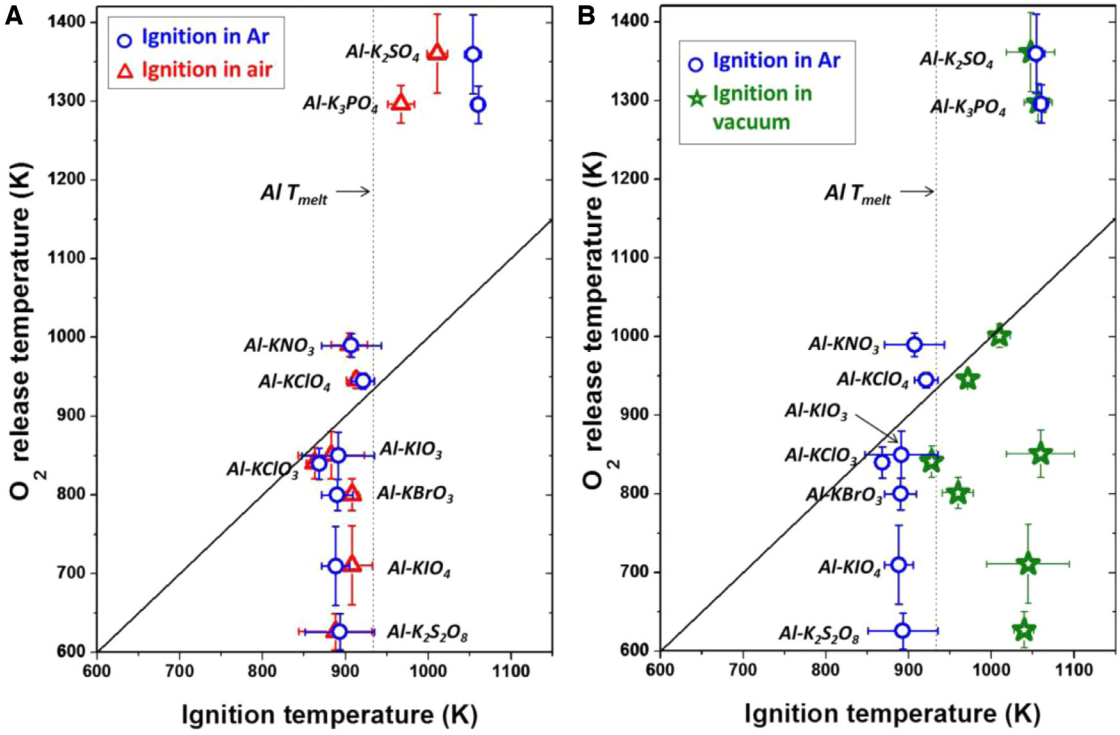

Fig. 3. (A) Relationship between the oxygen release temperature in neat microscale oxysalt, and the ignition temperature of corresponding nano-Al-fueled thermite in Ar or in air. (B) Relationship between the oxygen release temperature in neat microscale oxysalt, and the ignition temperature of corresponding nano-Al-fueled thermite in Ar or in vacuum. Each temperature test was repeated at least twice. The diagonal solid line stands for a perfect correlation. The vertical dashed line indicates the melting temperature of Al (933 K).

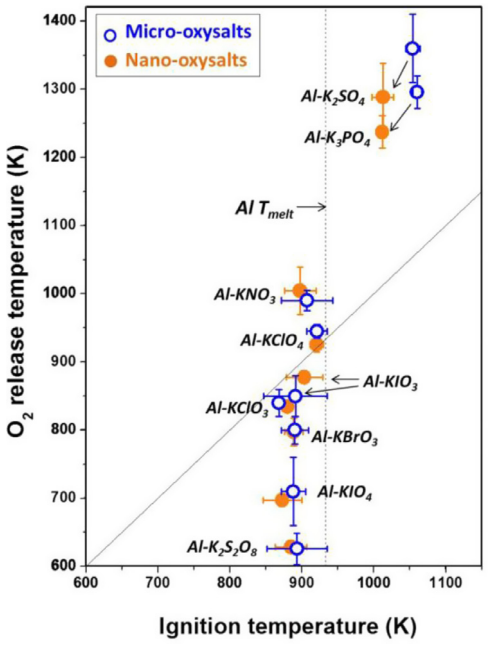

Fig. 4. Effect of particle size: relationship between the oxygen release temperature in neat nanoscale and microscale oxysalts, and the ignition temperature of corresponding nano-Al-fueled thermite in Ar. The arrows designate the temperature shifts of both ignition temperatures and oxygen release temperatures for Al–K_2SO_4 and Al–K_3PO_4 thermites when the dimension of oxysalt drops from micrometer scale to nanometer scale.

typical comparison of the O_2 release temperature and the ignition temperature between nano-Al/nano-oxysalt and nano-Al/micro-oxysalt thermites in Ar was conducted in Fig. 4. Compared with the nano-Al/micro-oxysalt thermites, the nano-Al/micro-oxysalt thermites of Al–K_2SO_4 and Al–K_3PO_4 show more than 50 K reduction both in O_2 release and ignition temperatures. Since both thermites follow a condense phase reaction mechanism, it is reasonable to see the decrease in these characteristic temperatures due to the increase of contact area between Al and oxysalt. In contrast, the ignition temperatures for the other seven thermites are independent of particle size, indicating that it is the reaction of Al and gaseous O_2 that contributes to the combustion initiation (Fig. 4).

Our proposed dual-phase reaction mechanism for reactive Al–oxysalts thermites, if correct, would provide a linear correlation between the ignition temperature and the relevant O_2 release temperature. However, since the Al fuel has a alumina shell that limits the transport of Al and O, the thermite ignition is largely influenced by the accelerated Al diffusion, based on the fact that ignition occurs near the melting point of the metallic aluminum core (Fig. 3). The ignition temperatures of the seven reactive Al–oxysalt thermites were close to the aluminum melting point in both Ar and air (Fig. 3A and Fig. S3A) even though the corresponding oxysalts have different O_2 release temperatures. This indicates that the ignition was controlled by the accelerated outward diffusion of aluminum. However, this result provides no indication as to the nature of the reactive oxygen species that reacts with Al. The fact that in vacuum, where we expect little gas phase oxygen to play a role, the ignition temperature increases suggests that the initiating mechanism transitions from an oxygen gas reaction to a condensed phase oxygen exchange process.

To further explore this point we employ carbon as a fuel, because unlike Al, it has a very high melting temperature, thus no fuel mobility (> 3800 K), and since there is no oxide shell, the fuel is directly accessible to the oxidizer. Figure 5 and Table S4 shows that in contrast to Al, where ignition was confined to near the melting point of Al regardless of oxidizer species, the reactive nano-carbon/micro-oxysalt thermites (Al–KNO_3, Al–$KClO_4$,

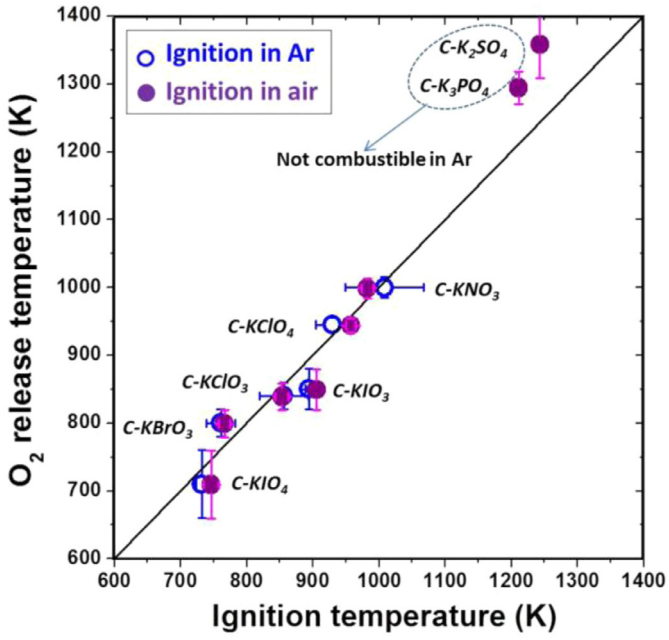

Fig. 5. Relationship between the oxygen release temperature in neat microscale oxysalt, and the ignition temperature of corresponding nano-carbon-fueled thermite in Ar or in air. Each temperature test was repeated at least twice. The diagonal solid line stands for a perfect correlation. C–K_2SO_4 and C–K_3PO_4 thermites were found to be not combustible in Ar, and thus the relevant ignition temperatures were vacant in the diagram.

Al–KIO_3, Al–$KClO_3$, Al–$KBrO_3$, and Al–KIO_4) have a near perfect linear correlation between ignition and O_2 release temperatures both in Ar and in air. These reactive thermites are incombustible in vacuum, probably due to a lower reactivity of C than Al. These results clearly indicate that the reactive oxygen that leads to ignition with the surface bound carbon is from the released molecular oxygen, thus confirming the Al–O_2(g) reaction mechanism for the reactive oxysalt-containing thermites.

Two exceptions are C–K_2SO_4 and C–K_3PO_4, which are not combustible in Ar, while have higher ignition temperatures than their O_2 release temperatures in air. This result confirms our previous interpretation that the less reactive thermites undergo a condense phase reaction mechanism.

3.5. Reaction mechanisms

Here we summarize the experimental results within a framework of some plausible mechanisms as illustrated in Fig 6. In this study we consider mainly four characteristic temperatures. The ignition temperature (T_{ig}), the oxygen release temperature (T_{O_2}), the phase change temperature for the alumina shell ($T_{\gamma-Al_2O_3}$, which is close to the melting temperature of aluminum, $T_{Al\text{-}melt}$), and the melting temperature of oxysalt ($T_{oxidizer\text{-}melt}$). The nine Al–oxysalt thermites can be generally divided into two groups. The first group includes Al–$K_2S_2O_8$, Al–KIO_4, Al–KIO_3, Al–$KClO_3$ and Al–$KBrO_3$ as they fall *below the diagonal* in Fig. 3A. These thermites have $T_{O_2} < T_{\gamma-Al_2O_3} = T_{ig} < T_{Al\text{-}melt}$, and minimal or lower $T_{oxidizer\text{-}melt}$. The ignition for these thermites is driven by the interaction of released O_2 from the oxysalt and the accelerated outwardly diffusing Al atoms when the temperature of the polymorphic phase change in

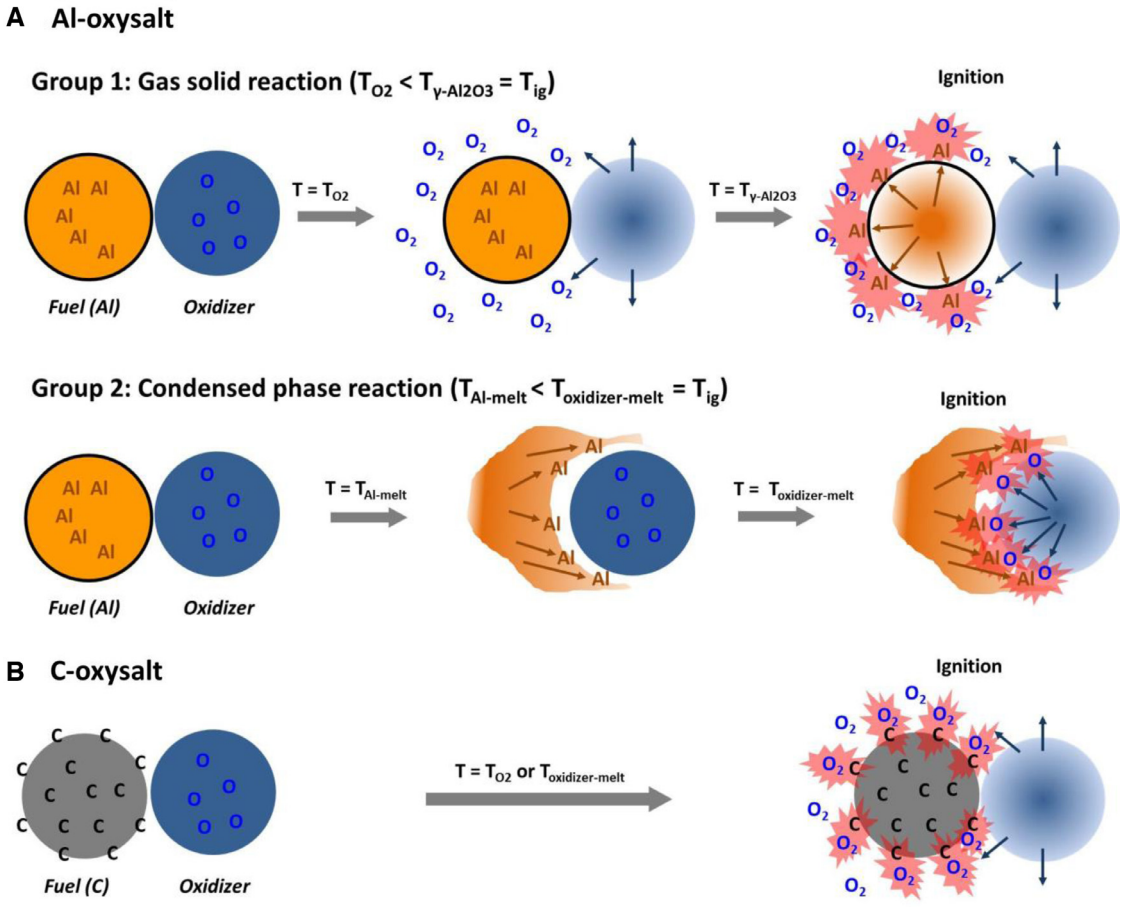

Fig. 6. Ignition mechanisms for the Al–oxysalt thermites (A) and C–oxysalt thermites (B).

alumina (~880 K, from amorphous to γ-Al_2O_3) is reached (which also approaches $T_{Al\text{-}melt}$ at ~930 K) [22]. This phase change at ~880 K features some degree of porosity in the alumina shell due to the increase of alumina density, leading to the enhancement of Al diffusion across the alumina shell, and therefore the initiation of thermite reaction. Two thermites including Al–KNO_3 and Al–$KClO_4$ have a transformed ignition type subordinate to the first group (Fig. S4), which ignite before oxygen is released. These are the thermites that are found *above the diagonal* in Fig. 3A. In this case, the oxysalt melts prior to ignition ($T_{oxidizer\text{-}melt} < T_{\gamma-Al_2O_3} = T_{ig} < T_{O_2}$), thus the thermite must initially be ignited by the interaction of bound oxygen in the molten oxysalt and accelerated outwardly diffused Al at the temperature of polymorphic phase change in the alumina shell (~880 K, close by $T_{Al\text{-}melt}$). Once ignition commences, self-heating will generate gaseous oxygen which then will be the predominant reaction mechanism, as the in-vacuum experiments illustrate (Fig. 3B). The second group of thermites includes Al–K_2SO_4 and Al–K_3PO_4 that are *substantially above the diagonal* (Fig. 3A) and thus gas-phase generated oxygen cannot be important. The ignition temperatures for these less reactive thermites are higher than $T_{Al\text{-}melt}$, while lower than T_{O_2} (Fig. 3A), suggesting that ignition is determined by the accelerated outward flow of oxygen from the melt oxysalt ($T_{Al\text{-}melt} < T_{oxidizer\text{-}melt} = T_{ig} < T_{O_2}$). These results demonstrate that ignition of Al–oxysalt thermites requires both the availability of Al and oxygen at the reaction interface, and is much related to the temperature of polymorphic phase change for alumina ($T_{\gamma-Al_2O_3}$). The first group of thermites has a lower temperature for oxygen availability (either T_{O_2} or $T_{oxidizer\text{-}melt}$) than $T_{\gamma-Al_2O_3}$, thus ignition for these formulations is triggered by the accelerated diffusion of Al ($T_{ig} = T_{\gamma-Al_2O_3}$). Conversely, the other group of thermites has a higher temperature for oxygen availability (mainly $T_{oxidizer\text{-}melt}$) than $T_{\gamma-Al_2O_3}$, thus the limiting step in triggering is the accelerated diffusion of oxygen ($T_{ig} = T_{oxidizer\text{-}melt}$).

For the ignition of nano-C with oxidizers, since carbon is solid and has no oxide shell at all the ignition temperatures, ignition is simply controlled by the availability of reactive oxygen from the oxidizers (decomposition or melting) (Fig. 6B). Thus, most of the ignition temperatures are linearly correlated to the relevant O_2 release temperature or melting temperature of oxidizers.

4. Conclusions

We implemented a study of the reaction mechanisms of oxysalt-containing thermites. Based on their combustion behavior, nine oxysalt-containing thermites were divided into two groups, with the reactive thermites (e.g., Al–$K_2S_2O_8$) showing ~10× higher maximum pressure, and ~10× shorter burn time than the less reactive thermites (e.g., Al–K_2SO_4). The difference in ignition temperature (T_{ig}) is attributed to the oxygen release temperature (T_{O_2}), the temperature of polymorphic phase change for alumina ($T_{\gamma-Al_2O_3}$), and the melting temperature of oxysalt ($T_{oxidizer\text{-}melt}$). The basic results are: (1) T_{ig} of the reactive thermites in Ar and in air are similar to $T_{\gamma-Al_2O_3}$ (close to $T_{Al\text{-}melt}$), while the corresponding T_{ig} in vacuum are higher; (2) T_{ig} of the less reactive thermites in Ar and in vacuum are consistent, and much higher than $T_{Al\text{-}melt}$, although lower than T_{O_2} and $T_{oxidizer\text{-}melt}$ of the corresponding oxysalts. These results indicate that the limiting initiation step of the reactive thermites is the capability of Al atoms to diffuse through the Al_2O_3 shell towards the reactive oxygen at the interface (gaseous or molten), whereas the limiting initiation step of the less reactive thermites is the decomposition or melting of oxysalts to deliver oxygen to the molten Al. Use of nano-carbon-fueled oxysalt thermites confirm that there are two reaction mechanisms for these oxysalt-containing thermites. In terms of the various ignition dependence of heterogeneous solid–gas reaction or condense state reaction, we proposed a general framework of ignition mechanisms for different oxysalt-containing thermites.

Acknowledgments

Financial support from DOD/DTRA (BRBAA08-Per5-H-2-0065) and the Army Research Office. Garth Egan for his thoughts and discussions on ignition mechanisms.

Supplementary materials

Supplementary material associated with this article can be found, in the online version, at doi:10.1016/j.combustflame.2016.05.024.

References

[1] H. Goldschmidt, New Thermite Reactions, Iron Age 82 (1908) 232.
[2] E.L. Dreizin, Metal-based reactive nanomaterials, Prog. Energy Combust. Sci. 35 (2009) 141–167.
[3] R.A. Yetter, G.A. Risha, S.F. Son, Metal particle combustion and nanotechnology, Proc. Combust. Inst. 32 (2009) 1819–1838.
[4] D.G. Piercey, T.M. Klapotke, Nanoscale aluminum-metal oxide (thermite) reactions for application in energetic materials, Central Euro. J. Energy Mater. 7 (2) (2010) 115–129.
[5] X. Zhou, M. Torabi, J. Lu, R. Shen, K. Zhang, Nanostructured energetic composites: synthesis, ignition/combustion modeling, and applications, ACS Appl. Mater. Interfaces 6 (2014) 3058–3074.
[6] Y. Li, J. Yao, Y. Liu, Synthesis and cladding of Al_2O_3 ceramic coatings on steel substrates by a laser controlled thermite reaction, Surf. Coat. Technol. 172 (2003) 57–64.
[7] E.B. Motlagh, J.V. Khaki, M.H. Sabzevar, Welding of aluminum alloys through thermite like reactions in Al–CuO–Ni system, Mater. Chem. Phys. 133 (2012) 757–763.
[8] P. Lynch, H. Krier, N. Glumac, A correlation for burn time of aluminum particles in the transition regime, Proc. Combust. Inst. 32 (2009) 1887–1893.
[9] J.C. Poret, A.P. Shaw, C.M. Csernica, K.D. Oyler, J.A. Vanatta, G. Chen, Versatile boron carbide-based energetic time delay compositions, ACS Sustain. Chem. Eng. 1 (2013) 1333–1338.
[10] K. Jayaraman, K.V. Anand, S.R. Chakravarthy, R. Sarathi, Effect of nano-aluminium in plateau-burning and catalyzed composite solid propellant combustion, Combust. Flame 156 (2009) 1662–1673.
[11] J. Bouillard, A. Vignes, O. Dufaud, L. Perrin, D. Thomas, Ignition and explosion risks of nanopowders, J. Hazard. Mater. 181 (2010) 873–880.
[12] B. Siegert, M. Comet, D. Spitzer, Safer energetic materials by a nanotechnological approach, Nanoscale 3 (2011) 3534–3544.
[13] L. Menon, S. Patibandla, K. Bhargava Ram, S.I. Shkuratov, D. Aurongzeb, M. Holtz, J. Berg, J. Yun, H. Temkin, Ignition studies of Al/Fe_2O_3 energetic nanocomposites, Appl. Phys. Lett. 84 (23) (2004) 4735–4737.
[14] C.E. Aumann, G.L. Skofronick, J.A. Martin, Oxidation behavior of aluminum nanopowders, J. Vac. Sci. Technol. B 13 (1995) 1178–1183.
[15] A.N. Pivkina, Y.V. Frolov, D.A. Ivanov, Nanosized components of energetic systems: structure, thermal behavior, and combustion, Combust. Exp. Shock Waves 43 (2007) 51–55.
[16] A.B. Morgan, J. Douglas Wolf, E.A. Guliants, K.A. Shiral Fernando, W.K. Lewis, Heat release measurements on micron and nano-scale aluminum powders, Thermochim. Acta 488 (2009) 1–9.
[17] Y. Li, R.K. Kalia, A. Nakano, P. Vashishta, Size effect on the oxidation of aluminum nanoparticle: multimillion-atom reactive molecular dynamics simulations, J. Appl. Phys. 114 (2013) 134312.
[18] K. Zhang, C. Rossi, P. Alphonse, C. Tenailleau, S. Cayez, J-Y. Chane-Ching, Integrating Al with NiO nano honeycomb to realize an energetic material on silicon substrate, Appl. Phys. A 94 (2009) 957–962.
[19] F. Severac, P. Alphonse, A. Esteve, A. Bancaud, C. Rossi, High-energy Al/CuO nanocomposites obtained by DNA-directed assembly, Adv. Funct. Mater. 22 (2012) 323–329.
[20] J.Y. Ahn, W.D. Kim, K. Cho, D. Lee, S.H. Kim, Effect of metal oxide nanostructures on the explosive property of metastable intermolecular composite particles, Powder Technol 211 (2011) 65–71.
[21] J.J. Granier, M.L. Pantoya, Laser ignition of nanocomposite thermites, Combust. Flame 138 (2004) 373–383.
[22] M.A. Trunov, M. Schoenitz, E.L. Dreizin, Combust. Effect of polymorphic phase transformations in alumina layer on ignition of aluminium particles, Theory Model. 10 (4) (2006) 603–623.
[23] A. Rai, K. Park, L. Zhou, M.R. Zachariah, Understanding the mechanism of aluminum nanoparticle oxidation, Combust. Theory Model. 10 (5) (2006) 843–859.
[24] M. Schoenitz, B. Patel, O. Agboh, E.L. Dreizin, Oxidation of aluminum powders at high heating rates, Thermochim. Acta 507-508 (2010) 115–122.
[25] S. Chowdhury, K. Sullivan, N. Piekiel, L. Zhou, M.R. Zachariah, Diffusive vs explosive reaction at the nanoscale, J. Phys. Chem. C 114 (20) (2010) 9191–9195.

[26] V.I. Levitas, B.W. Asay, S.F. Son, M. Pantoya, Melt dispersion mechanism for fast reaction of nanothermites, Appl. Phys. Lett. 89 (2006) 071909.
[27] V.I. Levitas, B.W. Asay, S.F. Son, M. Pantoya, Mechanochemical mechanism for fast reaction of metastable intermolecular composites based on dispersion of liquid metal, J. Appl. Phys. 101 (2007) 083524.
[28] V.I. Levitas, M. Pantoya, B. Dikici, Melt dispersion versus diffusive oxidation mechanism for aluminum nanoparticles: critical experiments and controlling parameters, Appl. Phys. Lett. 92 (2008) 011921.
[29] M.L. Pantoya, J.J. Granier, Combustion behavior of highly energetic thermites: nano versus micron composites, Propellants Explos. Pyrotech. 30 (2005) 53–62.
[30] G. Jian, S. Chowdhury, K. Sullivan, M.R. Zachariah, Nanothermite reactions: is gas phase oxygen generation from the oxygen carrier an essential prerequisite to ignition? Combust. Flame 160 (2013) 432–437.
[31] K. Sullivan, M.R. Zachariah, Simultaneous pressure and optical measurements of nanoaluminum thermites: investigating the reaction mechanism, J. Propul. Power 26 (3) (2010) 467–472.
[32] S.W. Dean, M.L. Pantoya, A.E. Gash, S.C. Stacy, L.J. Hope-Weeks, Enhanced convective heat transfer in nongas generating nanoparticle thermites, J. Heat Transf. 132 (2010) 111201.
[33] J.Z. Wen, S. Ringuette, G. Bohlouli-Zanjani, A. Hu, N.H. Nguyen, J. Persic, C.F. Petre, Y.N. Zhou, Characterization of thermochemical properties of Al nanoparticle and NiO nanowire composites, Nanoscale Res. Lett. 8 (2013) 184.
[34] K.T. Sullivan, W.A. Chiou, R. Fiore, M.R. Zachariah, In situ microscopy of rapidly heated nano-Al and nano-Al/WO_3 thermites, Appl. Phys. Lett. 97 (13) (2010) 133104.
[35] K.T. Sullivan, N.W. Piekiel, C. Wu, S. Chowdhury, S.T. Kelly, T.C. Hufnagel, K. Fezzaa, M.R. Zachariah, Reactive sintering: an important component in the combustion of nanocomposite thermites, Combust. Flame 159 (2012) 2–15.
[36] N.W. Piekiel, G.C. Egan, K.T. Sullivan, M.R. Zachariah, Evidence for the predominance of condensed phase reaction in chemical looping reactions between carbon and oxygen carriers, J. Phys. Chem. C 116 (2012) 24496–24502.
[37] N.W. Piekiel, L. Zhou, K.T. Sullivan, S. Chowdhury, G.C. Egan, M.R. Zachariah, Initiation and reaction in Al/Bi_2O_3 nanothermites: evidence for the predominance of condensed phase chemistry, Combust. Sci. Technol. 186 (2014) 1209–1224.
[38] R. Thiruvengadathan, A. Bezmelnitsyn, S. Apperson, C. Staley, P. Redner, W. Balas, S. Nicolich, D. Kapoor, K. Gangopadhyay, S. Gangopadhyay, Combustion characteristics of novel hybrid nanoenergetic formulations, Combust. Flame 158 (2011) 964–978.
[39] W.K. Lewis, B.A. Harruff, J.R. Gord, A.T. Rosenberger, T.M. Sexton, E.A. Guliants, C.E. Bunker, Chemical dynamics of aluminum nanoparticles in ammonium nitrate and ammonium perchlorate matrices: enhanced reactivity of organically capped aluminum, J. Phys. Chem. C 115 (2011) 70–77.
[40] S. Umbrajkar, M.A. Trunov, M. Schoenitz, E.L. Dreizin, Arrested reactive milling synthesis and characterization of sodium-nitrate based reactive composites, Propul. Explos. Pyrotech. 32 (2007) 32–41.
[41] M.A. Machado, D.A. Rodriguez, Y. Aly, M. Schoenitz, E.L. Dreizin, E. Shafirovich, Nanocomposite and mechanically alloyed reactive materials as energetic additives in chemical oxygen generators, Combust. Flame 161 (2014) 2708–2716.
[42] R.W. Armstrong, B. Bschung, D.W. Booth, M. Samirant, Enhanced propellant combustion with nanoparticles, Nano Lett. 3 (2003) 253–255.
[43] A.N. Pivkina, Y.V. Frolov, D.A. Ivanov, Nanosized components of energetic systems: structure, thermal behavior, and combustion, Combust. Exp. Shock Waves 43 (2007) 51–55.
[44] C. Wu, K. Sullivan, S. Chowdhury, G. Jian, L. Zhou, M.R. Zachariah, Encapsulation of perchlorate salts within metal oxides for application as nanoenergetic oxidizers, Adv. Funct. Mater. 22 (2012) 78–85.
[45] K.T. Sullivan, N.W. Piekiel, S. Chowdhury, C. Wu, M.R. Zachariah, C.E. Johnson, Ignition and combustion characteristics of nanoscale Al/$AgIO_3$: a potential energetic biocidal system, Combust. Sci. Technol. 183 (2011) 285–302.
[46] C.R. Becker, S. Apperson, C.J. Morris, S. Gangopadhyay, L.J. Currano, W.A. Churaman, C.R. Stoldt, Galvanic porous silicon composites for high-velocity nanoenergetics, Nano Lett. 11 (2011) 803–807.
[47] G. Jian, J. Feng, R.J. Jacob, G.C. Egan, M.R. Zachariah, Super-reactive nanoenergetic gas generators based on periodate salts, Angew. Chem. Int. Ed. 52 (2013) 9743–9746.
[48] A. Prakash, A.V. McCormick, M.R. Zachariah, Tuning the reactivity of energetic nanoparticles by creation of a core–shell nanostructure, Nano Lett. 5 (7) (2005) 1357–1360.
[49] A. Prakash, A.V. McCormick, M.R. Zachariah, Synthesis and reactivity of a super-reactive metastable intermolecular composite formulation of Al/$KMnO_4$, Adv. Mater. 17 (7) (2005) 900–903.
[50] W. Zhou, J.B. Delisio, X. Li, L. Liu, M.R. Zachariah, Persulfate salt as an oxidizer for biocidal energetic nano-thermites, J. Mater. Chem. A 3 (2015) 11838–11846.
[51] P.R.N. Childs, Practical temperature measurement, Butterworth Heinemann, London, U.K., 2001.
[52] L. Zhou, N. Piekiel, S. Chowdhury, M.R. Zachariah, Time-resolved mass spectrometry of the exothermic reaction between nano aluminum and metal oxides: the role of oxygen release, J. Phys. Chem. C 114 (2010) 14269–14275.
[53] K.H. Stern, High temperature properties and thermal decomposition of inorganic salts with oxyanions, CRC Press, Boca Raton, FL, 2007, p. 66.
[54] K.H. Stern, High temperature properties and thermal decomposition of inorganic salts with oxyanions, CRC Press, Boca Raton, FL, 2007, p. 148.
[55] M.E. Hagerman, V.L. Kozhevnikov, K.R. Poeppelmeier, High-temperature decomposition of potassium titanyl phosphate, $KTiOPO_4$, Chem. Mater. 5 (9) (1993) 1211–1215.